Received: 22 October 2018 | Revised: 3 January 2019 | Accepted: 3 March 2019

DOI: 10.1002/stc.2354

RESEARCH ARTICLE

WILEY

Real-time object detection using power spectral density of ground-penetrating radar data

Abolfazl Saghafi[1] | Sajad Jazayeri[2] | Sanaz Esmaeili[2] | Chris P. Tsokos[3]

[1]Department of Mathematics, Physics and Statistics, University of the Sciences, Philadelphia, Pennsylvania, USA

[2]School of Geosciences, University of South Florida, Tampa, Florida, USA

[3]Department of Mathematics and Statistics, University of South Florida, Tampa, Florida, USA

Correspondence
Sajad Jazayeri, School of Geosciences, University of South Florida, Tampa, FL 33620, USA.
Email: sjazayeri@mail.usf.edu

Summary

A statistical analytical monitoring scheme is developed that utilizes maximum energy of ground-penetrating radar signals to detect hidden buried objects and estimate their location and depth automatically. The maximum energy is calculated for locations by Welch's power spectral density estimation. Using the proposed analytic, the maximum energy is tightly monitored for a significant change from reference signals generated using target-free locations. A warning message is triggered when monitoring process detects a site with potential buried objects, on average, 90 cm (2.95 ft) away from the object for 800-MHz antenna. Continuing the ground-penetrating radar scan in the same direction and monitoring the signals, the procedure uses a sophisticated hyperbola-mapping method to estimate the location and depth of buried objects with high accuracy. The analytics could successfully pinpoint the location and depth of hidden objects, respectively, with mean absolute error of 0.38 and 2.03 cm in synthetic noisy environments. Reliable performance of the proposed analytics in real cases that run in real-time for multiple object detection even in noisy media proves its efficiency for real-life exploration.

KEYWORDS

detection, ground-penetrating radar, monitoring, power spectral density, sequential control process, utilities

1 | INTRODUCTION

Ground-penetrating radar (GPR) is very popular in the field of engineering for exploratory purposes due to its non-destructive utilization and fast data collection.[1,2] Manual processing of the accumulated data is time-consuming and requires experience. Besides, in many applications, for example, detecting rebar reinforcement in foundation construction, locating utilities, and detecting land mines and unexploded ordinance, abundance of possible targets could be extra challenging. To date, there have been various approaches aiming to automatize the object detection procedure. Wavelet transform,[3,4] Hough transform,[5-7] and Radon transform[8] are popular techniques among electrical engineering scholars.

Machine-learning techniques utilized by researchers in computer engineering are great assets in automatizing the object detection task. Neural networks and image processing-based pattern recognition methods are reported to be useful,[9-11] but they are sensitive to noise and fail to perform adequately in the presence of incomplete or highly disturbed hyperbolic patterns. Recently, Dou et al.[12] have proposed a column-connection-clustering algorithm to identify hyperbolic signatures, which again is successful if sharp and strong reflected signals are recorded. The reader is referred to Dou et al.[12] for a complete list of previously studied approaches.

Most recently, Jazayeri et al.[13] have proposed a statistical approach that measures dissimilarity of GPR signals to signals from target-free locations using dynamic time warping to detect burial sites. A hyperbola mapping is conducted on potential burial sites, which leads to highly accurate location, velocity, and depth estimation. Their method is proven to be reliable after testing with various synthetic and real-life data.

In this article, another statistical approach is introduced that is based on the fundamental idea of a signals's energy. The proposed method that runs automatically warns the user of potential burial sites by monitoring the energy of GPR signals. It performs automatic hyperbola mapping, location, velocity, and depth estimation with high accuracy. Moreover, the analytics run fast and are robust to low levels of noise, which make them suitable for on-site utilization. Considerable number of synthetic models are investigated using the proposed method as well as real data with striking results.

2 | MATERIALS

To statistically evaluate performance of the proposed method, 20 cases of synthetic models are generated in three scenarios. Scenario 1, with no buried object but signals, includes an additive noise and random outliers. Scenario 2, where a water-filled PVC pipe with wall thickness of 3 mm and inner diameter of 10 cm is buried in sand, in a random location and depth. Signals are free from noise and outliers in this scenario. In Scenario 3, additive noise is added to the cases in Scenario 2 to imitate more realistic models. The additive noise is considered to be a combination of white noise with Gaussian distribution, signal-to-noise ratio of 25 dB, and random outliers.[14,15] These 2D synthetic models are created using the finite difference–time domain gprMax code.[16,17] All materials are considered to be homogeneous (see Table 1). The transmitted pulse is an 800-MHz ricker, with the antenna offset of 14 cm and the trace interval of 2.5 cm.

In addition, to assess the performance of the proposed analytics in real life, two cases of real data are investigated. First, a data set was collected over a sand test site where multiple buried pipes and tree roots existed. A MALA ProEx GPR system with 800-MHz–shielded antenna was used to probe the ground where two PVC pipes with wall thickness of 3 mm and radius of 4.1 cm were buried in sand, 35 cm below the surface at 1.2 and 5.2 m. Beside the pipes, there were two pieces of tree roots at 7.8 and 9.1 m all with hyperbolic responses. Second, a portion of a long GPR profile collected on a road using the same system is utilized that illustrates a real complex environment. The study area is part of a main road covered with asphalt, embracing different utilities and drainage channels. All the synthetic and real data are available on the first author's website.

3 | METHODS

Power spectral density (PSD) of a signal refers to its spectral energy distribution as a function of frequency. The PSD has been used to diagnose faults in hydraulic pumps and electromotors,[18,19] to evaluate damage in concrete,[20] and to monitor machine conditions,[21] among others. When searching for hidden underground objects using GPR, the recorded signal is expected to be stronger in energy by approaching a buried object. This is because more signal waves are reflected to the receiver when they hit underground objects. Thus, it is logical that the energy of GPR signals change depending on the distance from buried objects. This idea in fact is used in this article to detect multiple buried objects. Figure 1 shows how a reference signal generated from a target-free location and a signal from a location directly above a buried object are different and how this affects their power spectral density estimate.

The Welch method is used in this article to estimate the PSD.[22,23] The general procedure behind Welch method is first to segment a signal $\boldsymbol{x} = (x_1, \ldots x_T)$ of length T into K-overlapped segments of size M. For each segment, then compute a windowed discrete Fourier transform at some frequency $\nu = j/M$ with $-(M/2 - 1) \leq j \leq M/2$:

$$X_k(\nu) = \sum_m x(m)w(m)\exp(-j2\pi\nu m), \quad m = (k-1)S, \ldots, M + (k-1)S - 1, \tag{1}$$

TABLE 1 Material properties

Media	Relative permittivity	Electrical conductivity (mS/m)
Soil	5	1
PVC pipe	3	1
Water	80	1

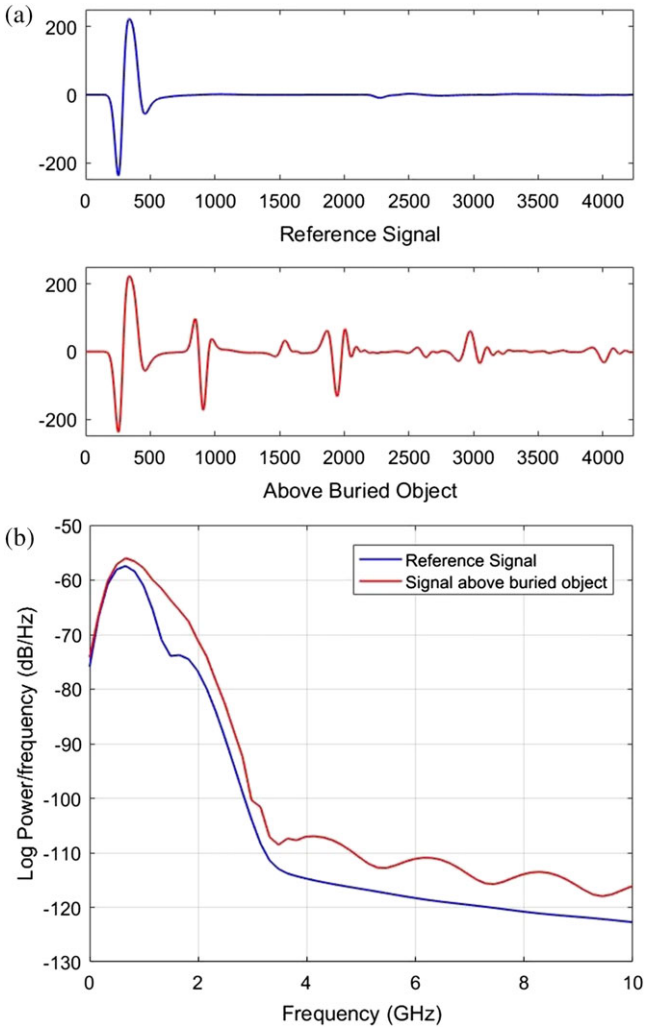

FIGURE 1 (a) Sample of a reference signal and a signal above buried object. (b) Welch power spectral density estimate

where S is the number of points to shift between segments and $w(m)$ is the Hamming window function. Next, compute the modified periodogram value from the discrete Fourier transform for each segment:

$$P_k(\nu) = \frac{1}{W}|X_k(\nu)|^2, \quad k = 1, .., K, \tag{2}$$

where $W = \sum_{m=1}^{M} w^2(m)$. Welch's estimate of the PSD is then obtained by averaging the periodogram values:

$$S_x(\nu) = \frac{1}{K}\sum_{k=1}^{K} P_k(\nu). \tag{3}$$

Figure 2 shows maximum PSD of Case no. 6 in the three discussed experimental scenarios along with their GPR profiles. Obviously, existence of a buried object is detectable using the maximum PSD because there is an increasing pattern to its values by approaching the object. The maximum energy of signals from target-free locations has a constant value with minor deviations due to noise. PSD is powerful to cancel out noise within the signal, see how results from Scenarios 2 and 3 have the same pattern with some deviations.

The general procedure to detect hidden buried objects using PSD is described below.

(a) Three target-free locations are scanned, and their GPR signal is recorded. These three signals serve as the initial reference signals for the current under investigation site.
(b) Proceed by scanning target areas and computing the maximum energy of the new locations using (3). The more similar the signals are to the reference signal, the closer their energy is. This also means that the ground is object free up to some fair distance.

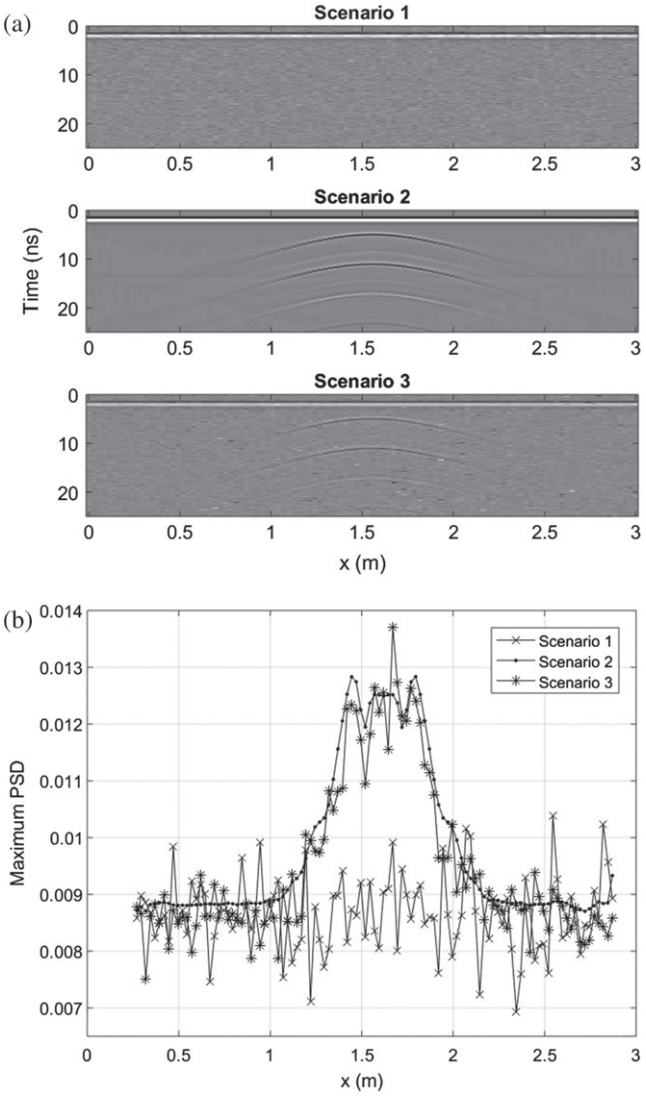

FIGURE 2 (a) Ground-penetrating radar profiles. (b) Maximum power spectral density for Case no. 6 in the three experimental scenarios

(c) By getting closer to a site with buried object(s), the max PSD value increases gradually. The potential burial site is close to where a peak of the max PSD happens. A more thorough investigation of neighboring locations uncovers a hyperbola signature, which is the key to location and depth estimation of the buried object(s).

In the next section, an explicit statistical approach is introduced to detect a buried object when approaching it while controlling the detection failure. The procedure is an online sequential control process that monitors GPR signals as they are being recorded. Repeating the same procedure on all local max PSD values is the key to multiple object detection.

4 | THEORY/CALCULATION

Suppose $\boldsymbol{x}_n = \left(x_n^1, x_n^2, \ldots, x_n^T\right)$ is the nth-recorded signal using GPR where $\boldsymbol{x}_1, \boldsymbol{x}_2$, and $\boldsymbol{x}_3$ are recorded from target-free locations. Assume p_n is the max PSD of the nth-recorded signal computed using (3). Let $\bar{p}_n^4$ represents the window average of the last four max PSD values given by

$$\bar{p}_n^4 = \frac{1}{4}\sum_{i=n-3}^{n} p_i, \tag{4}$$

and let $\bar{p}_n^{25}$ represents the window average of the last 25 max PSD values given by

$$\bar{p}_n^{25} = \frac{1}{25}\sum_{i=n-24}^{n} p_i, \tag{5}$$

where the average of 25 is computed for the available values in the beginning of the process and is shown by $\bar{p}_n^n$.

Theorem: As soon as the nth signal is recorded, the following decision boundary detects underground objects with probability of 0.999 for $n \geq 25$:

$$\bar{p}_n^4 > \bar{p}_n^{25} + u_n^{25}, \tag{6}$$

where

$$u_n^{25} = t_{(24,0.999)} s_n^{25} \left(\frac{21}{25^2}\right)\left(1 + \frac{21}{4^2}\right). \tag{7}$$

For $4 \leq n \leq 24$, the following boundary detects underground objects with the same probability:

$$\bar{p}_n^4 > \bar{p}_n^n + u_n^n, \tag{8}$$

where

$$u_n^n = t_{(n-1,0.999)} s_n^n \left(\frac{n-4}{n^2}\right)\left(1 + \frac{n-4}{n^2}\right). \tag{9}$$

The proof of the theorem is given in Appendix. The computational steps to use this theorem are as follows:

1. As soon as $\boldsymbol{x}_n$ ($n \geq 4$) is recorded, its maximum PSD is computed along with the window average of four $(\bar{p}_n^4)$ and the window average of 25 ($\bar{p}_n^{25}$ or $\bar{p}_n^n$ when applicable).
2. A one-sided t-student confidence interval $(0, \bar{p}_n^{25} + u_n^{25})$ is generated using (7). When there are less than 25 observations, this interval is computed as $(0, \bar{p}_n^n + u_n^n)$ using (9).
3. If $\bar{p}_n^4 \leq \bar{p}_n^{25} + u_n^{25}$ (or $\bar{p}_n^4 \leq \bar{p}_n^n + u_n^n$ when applicable), then process is under control, and the chance of failure in detection is 0.001. Otherwise, a warning is issued, and an object underground is detected ahead. In this case, the average $\bar{p}_n^4$ keeps increasing by approaching the buried object.
4. Scanning and monitoring target areas continue after a local peak of $\bar{p}_n^4$ is achieved. This peak happens around a highly probable burial site, $\boldsymbol{x}_n$ ($a \leq n \leq b$).
5. A hyperbola is tracked and mapped for signals of the probable burial site through analytic searching. The location of the buried object is estimated where the apex of the hyperbola happens.
6. A least-square approach is used to approximate the velocity using the marked nodes on the diffracted hyperbola in Step 5. Then, the one-way travel time of the wave at the estimated location of the target is multiplied by the velocity to estimate the depth. A zero-time correction is applied beforehand where the zero time is estimated using the potential burial site signals.
7. The process is repeated for all the local peaks of $\bar{p}^4$ for detecting multiple objects.

5 | RESULTS

Figure 3 shows the decision process using the proposed approach for Case no. 6 in the three discussed scenarios. In Scenario 1, where there was nothing underground, the confidence limit has some fluctuations. There are a few observations outside the confidence limit due to noise, which trigger a warning, but, overall, the change in max PSD is insignificant and does not create a significant peak of max PSD values. In Scenario 2, however, the confidence limit increases due to significant increase of signal's energy. Here, a warning alarm is generated at $x = 0.820$, the location and depth of the buried object are estimated to be 1.62 and 0.224 m, respectively. True location of the object was 1.62 m and 0.23 m underground. Scenario 3 generates roughly the same graph as Scenario 2 because PSD approach handles the additive noise quite well. An alarm is generated at $x = 0.395$, and the location and depth of the object are estimated to be 1.62 and 0.223 m, respectively.

Table 2 represents the overall performance of the 20 experimental cases in Scenarios 2 and 3. All 20 cases of Scenario 1 successfully generated a "nothing detected" notification whereas all cases in Scenarios 2 and 3 detected a hidden object. For cases in Scenario 2, a detection alarm generated at least 90 cm prior to reaching the object, on average. The mean absolute error (MAE) and root-mean-square error (RMSE) for location were 0.47 and 0.73 cm, respectively, meaning that on average, the error in estimating lateral location was 0.47 cm. The RMSE is a goodness of fit measure that includes both

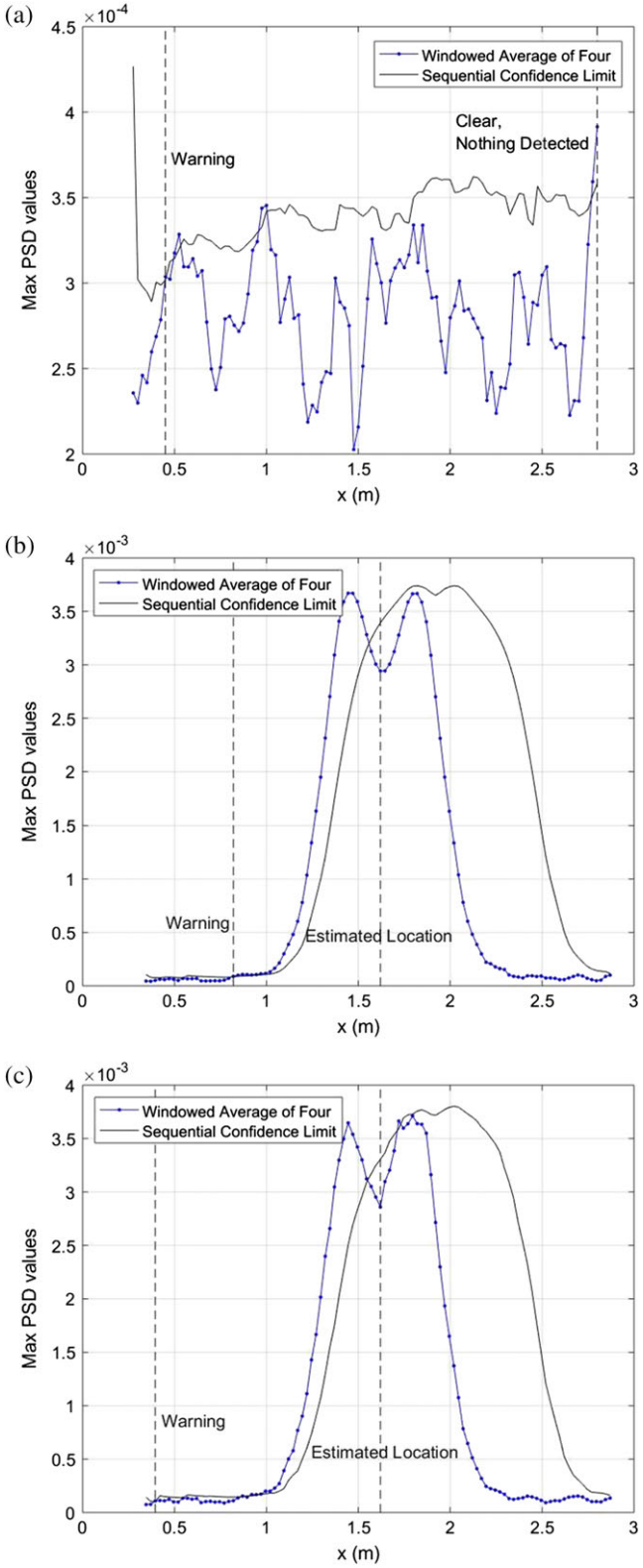

FIGURE 3 Maximum power spectral density control process for Case no. 6 in the three experimental scenarios: (a) Scenario 1, (b) Scenario 2, (c) Scenario 3

the estimation bias and variance. The depth in this scenario estimated with MAE of 1.80 and RMSE of 2.30 cm. For cases in Scenario 3, a detection alarm issued at least 94 cm ahead where the object was buried. The MAE and RMSE for location estimation were 0.375 and 0.602 cm, respectively. Depth estimation had a MAE of 2.027 cm and an RMSE of 2.837 cm.

TABLE 2 Mean absolute error (cm) and root-mean-square error (cm) of the max power spectral density analytics in 20 simulated cases for two scenarios

	Location			Depth	
Scenario	**Detection**	**MAE**	**RMSE**	**MAE**	**RMSE**
Scenario 2	89.975	0.474	0.725	1.797	2.299
Scenario 3	93.975	0.375	0.602	2.027	2.837

Note. MAE: mean absolute error; RMSE: root-mean-square error.

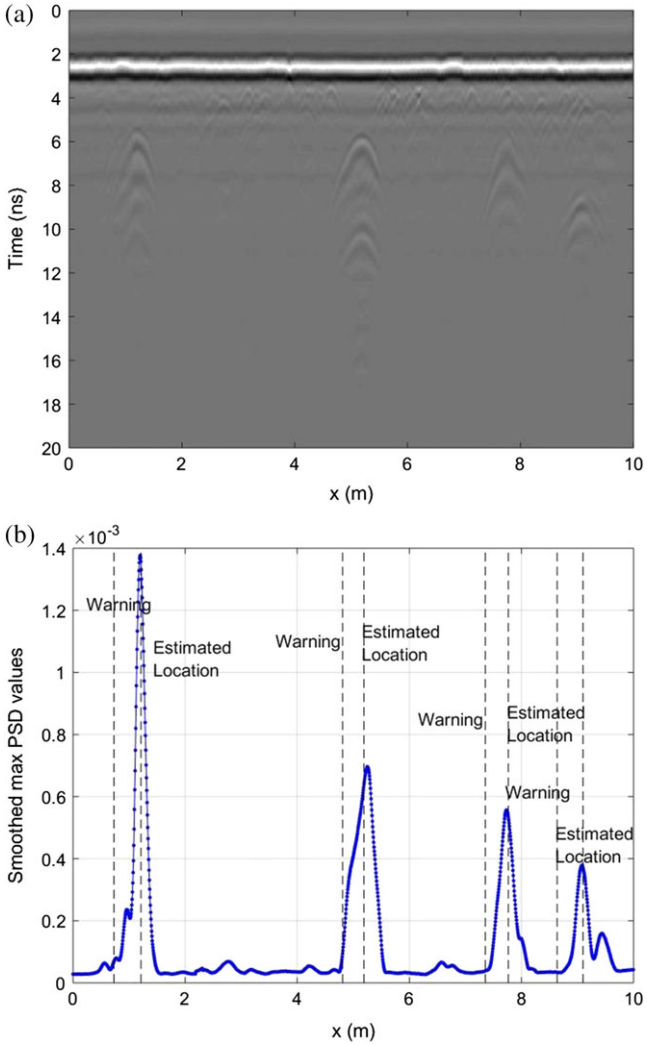

FIGURE 4 (a) Ground-penetrating radar profile collected over Geopark pipe site. (b) Smoothed max power spectral density values with warning and estimated locations

As expected, the proposed analytics performed quite well in real-life data with multiple buried objects. Figure 4 shows the profiles of the real data collected on pipes in sandy media and the smoothed max PSD values. The smoothing has been carried on using a moving average of 21 that was set by experimenting on the synthetic data. The location of the objects estimated to be $x = 1.216, 5.201, 7.761, 9.065$ m with corresponding depth of 0.353, 0.282, 0.387, and 0.430 m.

Figure 5 shows the GPR profile and smoothed max PSD values along with the generated warning and estimated locations for the second real data. The location and depth of the first object estimated to be 2.007 and 0.541 m, respectively. The second object estimated to be at 5.465 and 0.779 m underground. Performance of the analytics in this multiple object case is remarkable considering the level of distortion and noise in the data. To our experience, alternate detection methods[12] fail to detect the objects in this real case data due to severe existing distortions in the GPR signal. However, the proposed

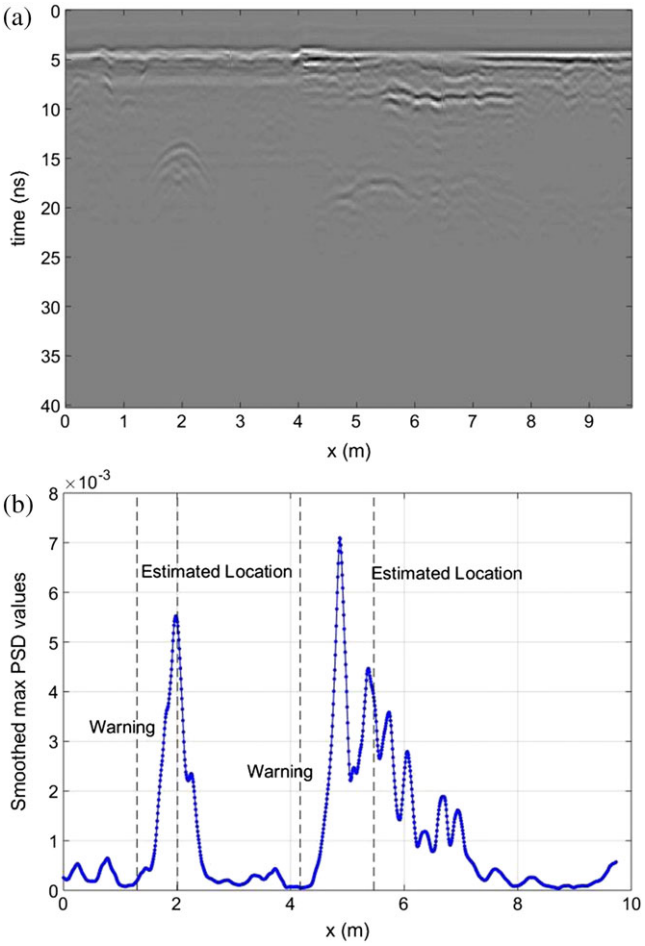

FIGURE 5 (a) Ground-penetrating radar profile collected on asphalt. (b) Smoothed max power spectral density values with warning and estimated locations

method successfully detects the objects and performs valid depth estimation using imperfect hyperbolic signatures. The exact locations and depths in this real experiment are unknown, but the results match expert expectations. There is a high sharp peak at 4.90 m in the smoothed max PSD plot that could be a result of mixed energies of two densely spaced anomalies. In this case, the analytics pick on the local max of the smoothed PSD values happening around 4.90 and track the trace of the hyperbola using a custom window search to reach its peak at 5.41 m. Three warnings are generated by the analytics at 1.29, 4.17, and 4.67 m, but hyperbola fitting results for the last two warnings converged, and one object was reported back.

Statistical measures such as MAE and RMSE computed over many samples are presented in this article that validate the reliability of the estimations. The main performance measure reported by other articles is the detection accuracy, which is calculated as the percent of correct object detections. To that extent, the proposed method in this paper had 100% success in detecting the subsurface anomalies in all cases of synthetic and real data used in this research. To our knowledge, the recent approach by Dou et al[12] fails to locate the drainage channel at 5.5 m whereas our analytics perform valid location and depth estimation beside the detection.

6 | CONCLUSIONS AND DISCUSSION

In this study, a statistical analytical monitoring scheme is proposed that utilizes maximum energy of GPR signals to detect multiple hidden buried objects and estimate their location as well as their depth. The computations run instantly and could be performed in real time. The synthetic and real data used in this article are accessible via the first author's personal home page*.

*AbolfazlSaghafi.info

An alarm is set to warn the user when a potential burial site is detected ahead by setting a threshold on the max PSD values. The site could be detected at least 44 cm ahead on average, and the threshold was set using *t*-student distribution. Sensitivity of the alarm process could be changed by changing the threshold.

A window average of four max PSDs for checking in/out of control states is utilized because four samples cut the length of the interval in half. The next window size that has significant effect on the length is nine, which is too much to consider. A window average of 25 max PSDs has been used to create confidence limits by considering the central limit theorem and approximate *t* distribution for the average. We are currently working on developing the analytics to detect multiple objects buried more closely.

ACKNOWLEDGEMENT

The authors are grateful to two anonymous reviewers for their constructive comments.

ORCID

Abolfazl Saghafi https://orcid.org/0000-0001-9535-9726
Sajad Jazayeri https://orcid.org/0000-0001-7441-5645
Sanaz Esmaeili https://orcid.org/0000-0002-6365-5587

REFERENCES

1. Benedetto A, Pajewski L. *Civil Engineering Applications of Ground Penetrating Radar*. Springer; 2015.
2. Jazayeri S, Klotzsche A, Kruse S. Improved resolution of pipes with full waveform inversion of common-offset GPR data using PEST. *Geophysics*. 2018;83(4):H27-H41. https://doi.org/10.1190/geo2017-0617.1
3. Hui-lin Z, Mao T, Xiao-li C. Feature extraction and classification of echo signal of ground penetrating radar. *Wuhan Univ J Nat Sci*. 2005;10(6):1009-1012.
4. Lu Q, Pu J, Liu Z. Feature extraction and automatic material classification of underground objects from ground penetrating radar data. *J Electr Comput Eng*. 2014;2014:28.
5. Windsor CG, Capineri L, Falorni P. The estimation of buried pipe diameters by generalized Hough transform of radar data. *PIERS Online*. 2005;1(3):345-349.
6. Qiao L, Qin Y, Ren X, Wang Q. Identification of buried objects in GPR using amplitude modulated signals extracted from multiresolution monogenic signal analysis. *Sensors*. 2015;15(12):30340-30350.
7. Li W, Cui X, Guo L, Chen J, Chen X, Cao X. Tree root automatic recognition in ground penetrating radar profiles based on randomized Hough transform. *Remote Sens*. 2016;8(5):430.
8. Dell'Acqua A, Sarti A, Tubaro S, Zanzi L. Detection of linear objects in GPR data. *Signal Process*. 2004;84(4):785-799.
9. Al-Nuaimy W, Huang Y, Nakhkash M, Fang M, Nguyen V, Eriksen A. Automatic detection of buried utilities and solid objects with GPR using neural networks and pattern recognition. *J Appl Geophys*. 2000;43(2):157-165.
10. Birkenfeld S. Automatic detection of reflexion hyperbolas in GPR data with neural networks. In: World Automation Congress (WAC), 2010 IEEE; 2010; Kobe, Japan:1-6.
11. Maas C, Schmalzl J. Using pattern recognition to automatically localize reflection hyperbolas in data from ground penetrating radar. *Comput Geosci*. 2013;58:116-125.
12. Dou Q, Wei L, Magee DR, Cohn AG. Real-time hyperbola recognition and fitting in GPR data. *IEEE Trans Geosci Remote Sens*. 2017;55(1):51-62.
13. Jazayeri S, Saghafi A, Esmaeili S, Tsokos CP. Online object detection using dynamic time warping on common-offset GPR. *Expert Syst Appl*. 2019;122:102-107.
14. Jazayeri S, Kazemi N, Kruse S. Sparse blind deconvolution of ground penetrating radar data. *IEEE Trans Geosci Remote Sens*. 2018. https://doi.org/10.1109/TGRS.2018.2886741
15. Jazayeri S, Ebrahimi A, Kruse S. Sparse blind deconvolution of common-offset GPR data. *SEG Technical Program Expanded Abstracts 2017*. Houston, Texas: Society of Exploration Geophysicists; 2017:5140-5145.
16. Warren C, Giannopoulos A, Giannakis I. gprMax open source software to simulate electromagnetic wave propagation for ground penetrating radar. *Comput Phys Comm*. 2016;209:163-170.
17. Jazayeri S, Kruse S, Hasan I, Yazdani N. Sparse blind deconvolution and full-waveform inversion of surface GPR data, an engineering example. *SEG Technical Program Expanded Abstracts 2018*. Anaheim, California, USA; 2018:5482-5486.
18. Ahmadi H, Khaksar Z. Using power spectral density for fault diagnosis of belt conveyor electromotor. *Innovative Computing Technology*. Berlin, Heidelberg: Springer; 2011:15-20.
19. Mollazade K, Ahmadi H, Omid M, Alimardani R. An intelligent combined method based on power spectral density, decision trees and fuzzy logic for hydraulic pumps fault diagnosis. *Int J Intell Syst Technol*. 2008;3(4):251-263.
20. Rucka M, Wilde K. Ultrasound monitoring for evaluation of damage in reinforced concrete. *Bull Pol Acad Sci Tech Sci*. 2015;63(1):65-75.

21. Moosavian A, Ahmadi H, Tabatabaeefar A. Condition monitoring of engine journal bearing using power spectral density and support vector machine. *Elixir Int J*. 2012;43:6631-6635.
22. Solomon OJr. PSD computations using Welch's method. NASA STI/Recon Technical Report N 92; 1991.
23. Parhi KK, Ayinala M. Low-complexity Welch power spectral density computation. *IEEE Trans Circuits Syst I Reg Papers*. 2014;61(1):172-182.

How to cite this article: Saghafi A, Jazayeri S, Esmaeili S, Tsokos CP. Real-time object detection using power spectral density of ground-penetrating radar data. *Struct Control Health Monit*. 2019;e2354. https://doi.org/10.1002/stc.2354

APPENDIX A: PROOF OF THEOREM

The proof is provided for $n \geq 25$; steps are similar for $4 \leq n \leq 24$. Under the hypothesis that there is nothing underground, the window average of 25 and four has the same expected value, that is,

$$E\left(\bar{P}_n^4\right) = \mu^4 = \mu^{25} = E\left(\bar{P}_n^{25}\right).$$

However, by approaching target locations, the window average of four increases promptly whereas the window average of 25 increases gradually. To detect this change as quickly as possible, we are testing the following statistical hypothesis at each step of the process:

$$H_0 : \mu^4 = \mu^{25} \quad Vs \quad H_1 : \mu^4 > \mu^{25},$$

where μ^4 is the true mean of the window average of four max PSD values and μ^{25} is the mean of the window average of 25 max PSD. The test statistic is $(\bar{P}_n^4 - \bar{P}_n^{25})$, which is unbiased under null hypothesis:

$$E\left(\bar{P}_n^4 - \bar{P}_n^{25}\right) = 0,$$

and has the following variance

$$Var\left(\bar{P}_n^4 - \bar{P}_n^{25}\right) = \sigma^2\left(\frac{21}{25^2}\right)\left(1 + \frac{21}{4^2}\right),$$

where $Var\left(\bar{P}_n^n\right) = \sigma^2/n$. Thus, using central limit theorem, one has

$$\frac{\left(\bar{P}_n^4 - \bar{P}_n^{25}\right)}{\sigma^2\left(\frac{21}{25^2}\right)\left(1 + \frac{21}{4^2}\right)} \approx N(0,1).$$

By estimating σ^2 using the last 25 observations, we have

$$\frac{\left(\bar{P}_n^4 - \bar{P}_n^{25}\right)}{s_n^{25}\left(\frac{21}{25^2}\right)\left(1 + \frac{21}{4^2}\right)} \approx t_{(n-1)},$$

where

$$s_n^{25} = \sqrt{\frac{1}{24}\sum_{i=n-24}^{n}\left(p_i - \bar{p}_n^{25}\right)^2}.$$

Thus, using a t-distribution confidence interval, when an object is buried underground, we have $\left(\bar{p}_n^4 - \bar{p}_n^{25}\right) > u_n^{25}$, where

$$u_n^{25} = t_{(24,0.999)}s_n^{25}\left(\frac{21}{25^2}\right)\left(1 + \frac{21}{4^2}\right).$$

As long as $\left(\bar{p}_n^4 - \bar{p}_n^{25}\right) \leq u_n^{25}$, the process is under control, and the probability of not detecting a change equals 0.001, which is related to the selected t-distribution critical value.